JOURNAL OF MATERIALS SCIENCE 30 (1995) 3319–3332

Microstructural modelling of auxetic microporous polymers

A. ALDERSON
Department of Materials Science and Engineering, University of Liverpool, P.O. Box 147, Liverpool L69 3BX, UK

K. E. EVANS*
School of Engineering, University of Exeter, North Park Road, Exeter EX4 4QF, UK

A simple two-dimensional model for the deformation of auxetic microporous polymers (those with a negative Poisson's ratio) has been developed. This model network of rectangular nodules interconnected by fibrils has been further developed to include the possibilities of fibril hinging, flexure and stretching. Expressions for strain-dependent Poisson's ratio and Young's modulus have been derived and compared with experimental results on microporous PTFE and UHMWPE. A combination of the hinging mode followed by the stretching mode of deformation can be used to explain the general features of the experimental data for these auxetic polymers. The force coefficients governing the different modes of deformation are dependent on fibril dimensions and intrinsic material properties. By varying the geometry of the network, the model can be used to predict different combinations of Poisson's ratio with modulus, from large positive through to large negative values.

1. Introduction

An increasing number of materials are now known to exhibit a negative Poisson's ratio, that is, they expand laterally in response to a longitudinal tensile load. Termed "auxetic materials" [1], the mechanisms responsible for the negative Poisson's ratio effect can act on an atomic or molecular level, as is the case for the α-cristobalite polymorph of crystalline silica [2–4], or on a larger microstructural scale in, for example, microporous polymers [5–7] and, on a larger scale, in auxetic foams [8, 9]. Potential benefits of auxetic materials include increased fracture toughness, enhanced indentation resistance [8, 10, 11] and improved drapability [12].

In the case of microporous polymeric materials, there are published experimental data for auxetic forms of polytetrafluoroethylene (PTFE) [5] and ultra-high molecular weight polyethylene (UHMWPE) [13, 14] showing strain-dependent behaviour. The microstructures of these polymers consist of a network of nodules of material interconnected by fibrils. The arrangement of the nodules and fibrils determines whether or not the Poisson's ratio is negative or positive. A simple geometric node–fibril (NF) model has been developed to interpret these data [13–15] consisting of rigid rectangular nodes connected by freely hinged inextensible rods. The model has been found to reproduce some of the features of the Poisson's ratio behaviour with strain, although the deformation over the total strain range covered experimentally has so far been unexplained by the model.

In this work, the NF model has been extended to allow the flexure and stretching as well as hinging of the fibrils. Expressions for Poisson's ratio and Young's modulus are derived for each mode of deformation and the behaviour of these mechanical properties with geometry is discussed and compared with the appropriate experimental data.

2. The node–fibril model for auxetic microporous polymers

The tensile NF network model for microporous PTFE is shown schematically in Fig. 1a. The rectangular nodules (major and minor axis lengths a and b, respectively, with the major axis aligned along the x direction) have previously [6] been considered to be connected by freely hinged, inextensible rods (fibrils) of length, l, at an angle, α, to the x axis. Under a tensile stress in the x direction, the fibrils hinge, thereby reducing the value of α until $\alpha = 0°$ is reached. Consequently, the nodules move apart in both the x and y directions, and the structure exhibits a negative Poisson's ratio. In this work the NF model has been developed to describe the Young's moduli as well as Poisson's ratios for the hinging model. It was further

*To whom correspondence should be addressed.

0022–2461

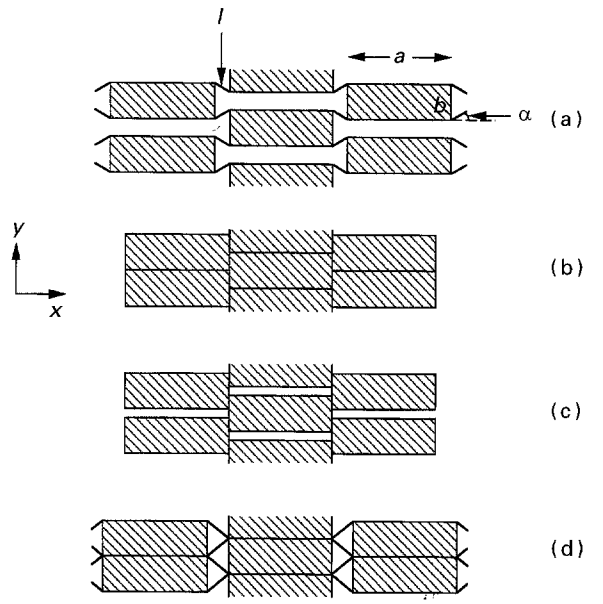

Figure 1 Schematic diagram of the nodule–fibril (NF) model, showing (a) general parameters in a partially extended network, (b) fully densified network with $l = b/2$, $\alpha_0 = 90°$, and undeformed, partially open networks resulting from (c) $l < b/2$, (d) $l > b/2$.

extended to describe fibril stretching and flexing. The model was then used to interpret both the Young's modulus and Poisson's ratio data for PTFE and UHMWPE, including the large variations in these properties with strain.

To obtain the Young's modulus from this model some form of elastic deformation process must be included. A previous approach [15] incorporated a separate independent set of springs between the nodules. A more realistic approach embodies the deformation mechanism into the fibrils themselves. The fibrils and nodules are of the same material but the fibrils can have a wide range of modulus as a result of the fabrication process, producing different draw ratios. If the nodules and fibrils have similar moduli, then deformation will be predominantly due to fibril stretching or flexing. If the fibrils have a much larger modulus than the nodules, fibril hinging will occur with local deformation of the nodule material at the base of the fibrils. For each mode of deformation we consider a force coefficient K_i where i represents the deformation mode. K can then be related to the intrinsic material parameters. Using the normal convention, the force coefficients employed in this paper are defined by

$$\Delta P_i = K_i \Delta x_i \quad (1)$$

where for linear displacements ΔP_i is the change in force F and Δx_i is the change in length x, and for angular displacements ΔP_i is the change in applied moment M and Δx_i is the change in the appropriate angle θ.

2.1. Fibril hinging

In this first model, the fibrils are considered to be inflexible rods, free to rotate. The Poisson's ratio, ν_{xy}, under a load in the x direction for the NF model (Fig. 1a) has been found to be [6]

$$\nu_{xy} = \frac{-\cos\alpha(a + l\cos\alpha)}{\sin\alpha(b - l\sin\alpha)} \quad (2)$$

The unit-cell lengths for the NF model are

$$X = 2(a + l\cos\alpha) \quad (3)$$

$$Y = 2(b - l\sin\alpha) \quad (4)$$

and the undeformed lengths are given by substituting the initial angle α_0 for α in Equations 3 and 4. Following the procedure outlined by Evans and Caddock [6] the engineering Poisson's ratio, ν^e_{xy} (i.e. related to the initial unit-cell lengths) is easily shown to be

$$\nu^e_{xy} = \frac{-\cos\alpha(a + l\cos\alpha_0)}{\sin\alpha(b - l\sin\alpha_0)} \quad (5)$$

For the Young's moduli of this structure, we consider a hinging force coefficient K_h, where, from Equation 1 (i = h), we have

$$l\Delta F = K_h \Delta\alpha \quad (6)$$

The left-hand side of Equation 6 is the change, ΔM, in the applied moment, M, to the fibril of length, l, due to a change ΔF, in the force, F, applied perpendicular to the end of the fibril. $\Delta\alpha$ is the angular displacement of the fibril due to the change in the applied moment – see Fig. 2.

Consider a unit thickness of the unit cell perpendicular to the x–y plane (Fig. 1a). The change, ΔF_x, in the applied load due to a change, $\Delta\sigma_x$, in the applied stress in the x direction is

$$\Delta F_x = \Delta\sigma_x Y \quad (7)$$

and hence the change, ΔF, in the perpendicular force, F, applied to each fibril is

$$\Delta F = \Delta F_x \sin\alpha/2 = \Delta\sigma_x Y \sin\alpha/2 \quad (8)$$

The change in X due to hinging under a small change, ΔF_x, in the applied load is

$$\Delta X = 2\Delta h \sin\alpha = 2l\Delta\alpha\sin\alpha \quad (9)$$

where Δh is the (small) displacement of the end of each fibril during hinging. From Equations 6 and 8

$$\Delta\alpha = l\Delta\sigma_x Y \sin\alpha/2K_h \quad (10)$$

In the limit of infinitesimal increments in applied stress, Equation 9 becomes

$$dX = d\sigma_x Y l^2 \sin^2\alpha/K_h \quad (11)$$

The Young's modulus in the x direction, E_x, at any given strain, ε_x, during a non-linear elastic deformation is defined as

$$E_x = d\sigma_x/d\varepsilon_x \quad (12)$$

where $d\varepsilon_x$ is an infinitesimal strain increment due to an infinitesimal increment in applied stress, $d\sigma_x$. For linear elasticity, Equation 12 is equivalent to $E_x = \sigma_x/\varepsilon_x$ and is constant. However, for strain-dependent non-linear elastic behaviour, the two expressions yield different values; in this case, Equation 12

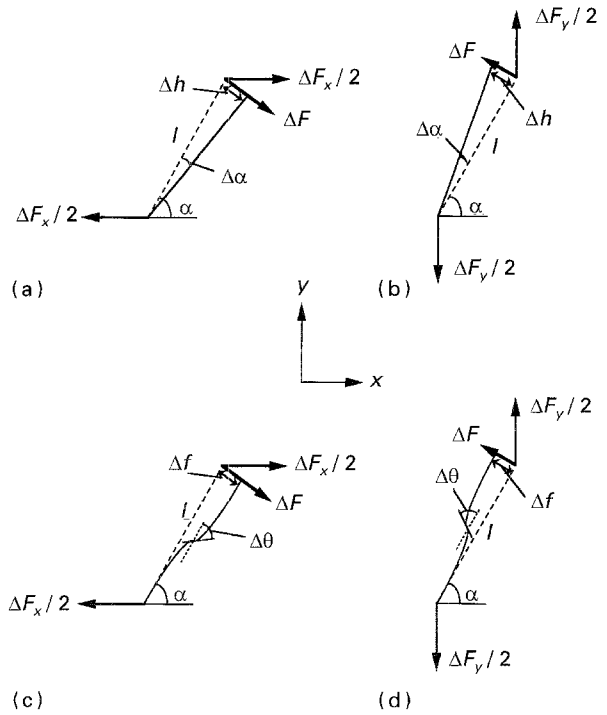

Figure 2 (a) Fibril hinging under tension of the NF network in the x direction. (b) Fibril hinging under compression of the NF network in the y direction. (c) Fibril flexure under tension of the NF network in the x direction. (d) Fibril flexure under compression of the NF network in the y direction.

(the tangent modulus) is the correct expression to use [16, 17]. $d\varepsilon_x$ is defined as

$$d\varepsilon_x = dX/X \tag{13}$$

From Equations 3, 4, 11–13, the Young's modulus in the x direction for the NF model is

$$E_x = \frac{K_h}{l^2 \sin^2\alpha} \frac{(a + l\cos\alpha)}{(b - l\sin\alpha)} \tag{14}$$

The engineering Young's modulus, E_x^e, is obtained by substituting the original unit-cell lengths X_0 and Y_0 for X and Y, respectively, in Equations 11 and 13, giving

$$E_x^e = \frac{K_h}{l^2 \sin^2\alpha} \frac{(a + l\cos\alpha_0)}{(b - l\sin\alpha_0)} \tag{15}$$

The expression for Poisson's ratio due to a load in the y direction for the NF model has been derived as [15]

$$\nu_{yx} = \frac{-\sin\alpha(b - l\sin\alpha)}{\cos\alpha(a + l\cos\alpha)} \tag{16}$$

and the engineering Poisson's ratio is

$$\nu_{yx}^e = \frac{-\sin\alpha(b - l\sin\alpha_0)}{\cos\alpha(a + l\cos\alpha_0)} \tag{17}$$

In this case the component of force causing fibril hinging is (see Fig. 2b)

$$\Delta F = \Delta F_y \cos\alpha/2 = \Delta\sigma_y X \cos\alpha/2 \tag{18}$$

where $\Delta\sigma_y$ is the change in the applied stress in the y direction. The change in Y due to hinging is

$$\Delta Y = 2\Delta h \cos\alpha = 2l\Delta\alpha\cos\alpha \tag{19}$$

where Δh is the (small) displacement of the end of each fibril during hinging. From Equations 6 and 18

$$\Delta\alpha = l\Delta\sigma_y X \cos\alpha/2K_h \tag{20}$$

Therefore, in the limit of infinitesimal increments in applied stress, Equation 19 becomes

$$dY = d\sigma_y X l^2 \cos^2\alpha/K_h \tag{21}$$

and hence the Young's modulus in the y direction in this case is

$$E_y = d\sigma_y/d\varepsilon_y = \frac{K_h}{l^2\cos^2\alpha} \frac{(b - l\sin\alpha)}{(a + l\cos\alpha)} \tag{22}$$

The engineering Young's modulus in the y direction is then

$$E_y^e = \frac{K_h}{l^2\cos^2\alpha} \frac{(b - l\sin\alpha_0)}{(a + l\cos\alpha_0)} \tag{23}$$

All these expressions are equally valid in tension or compression.

For an orthotropic material, the condition of a symmetric stiffness matrix requires [18]

$$\nu_{xy} E_y = \nu_{yx} E_x \tag{24}$$

Also, the requirement that the strain energy of an orthotropic material be positive definite for static equilibrium leads to [18]

$$|\nu_{xy}| \leq (E_x/E_y)^{1/2} \tag{25}$$

From Equations 2, 14, 16 and 22 we have

$$\nu_{xy} E_y = \nu_{yx} E_x = -K_h/l^2 \sin\alpha\cos\alpha \tag{26}$$

and

$$|\nu_{xy}| = (E_x/E_y)^{1/2} \tag{27}$$

Hence the NF model satisfies the requirements of a symmetric stiffness matrix (Equation 24) and a positive definite strain energy (Equation 25) for deformation due to hinging of the fibrils if the fibrils are considered to be inextensible rods.

Table I contains the relevant expressions for the elastic moduli (including the engineering moduli) due to hinging.

2.2. Fibril flexure

We now derive expressions for the Poisson's ratios and Young's moduli in the NF model by considering the fibrils as inextensible but flexible rods. We shall assume that the shear deformation of the rods can be neglected as can deformation of the nodules. This is valid for all fibril aspect ratios so far observed [5, 7]. The analysis closely follows the approach adopted in

the derivation of the elastic properties of two-dimensional honeycombs due to flexure of the cell walls [19].

Consider flexure of a fibril in the NF model (length l, fibril angle, α) under a change, $\Delta\sigma_x$, in a tensile load in the x direction (Fig. 2c). Using Equation 1 the flexure force coefficient, K_f, is defined as

$$K_f = \Delta M/\Delta\theta \tag{28}$$

where ΔM is the change in the bending moment M applied to the fibril and $\Delta\theta$ is the small change (i.e. $\Delta\theta = \tan\Delta\theta$) in the slope of the midpoint of the fibril with respect to the fibril orientation (see Fig. 2c). The change in the bending moment applied to the fibril is

$$\Delta M = \Delta F l/2 \tag{29}$$

where

$$\Delta F = \Delta F_x \sin\alpha/2 \tag{30}$$

and ΔF_x is given by Equation 7. From standard beam theory [20]

$$\Delta\theta = \frac{\Delta F(l/2)^2}{2E_s I} \tag{31}$$

where E_s is the intrinsic material Young's modulus and I is the second moment of inertia of the beam (fibril). The deflection, Δf, of the fibril due to flexure (see Fig. 2c) is given by

$$\Delta f = \frac{2\Delta F(l/2)^3}{3E_s I} \tag{32}$$

Hence from Equations 31 and 32

$$\Delta\theta = 3\Delta f/2l \tag{33}$$

Substituting Equations 7, 29, 30 and 33 into Equation 28 we find

$$\Delta f = \frac{\Delta\sigma_x Y l^2 \sin\alpha}{6K_f} \tag{34}$$

The changes in the unit-cell lengths due to deflection of the fibrils in flexure at angle, α, are

$$\Delta X = 2\Delta f \sin\alpha \tag{35}$$

$$\Delta Y = 2\Delta f \cos\alpha \tag{36}$$

In the limit of infinitesimal unit length changes the infinitesimal changes in strain are, therefore

$$d\varepsilon_x = 2df\sin\alpha/X \tag{37}$$

$$d\varepsilon_y = 2df\cos\alpha/Y \tag{38}$$

where X and Y are given by Equations 3 and 4, respectively. The infinitesimal changes in engineering strain are found by substituting the initial unit-cell lengths X_0 and Y_0 for X and Y, respectively, in Equations 37 and 38. For the same reason that Equation 12 is the correct definition of Young's modulus for a non-linear deformation, the Poisson's ratio due to a uniaxial applied stress along the x direction for non-linear elastic behaviour, referred to as Poisson's function, is defined [16, 21] as

$$\nu_{xy} = -d\varepsilon_y/d\varepsilon_x \tag{39}$$

Hence, we find for deformation of the node–fibril network due to flexure of the fibrils at an angle, α, to the x axis

$$\nu_{xy} = \frac{-\cos\alpha(a + l\cos\alpha)}{\sin\alpha(b - l\sin\alpha)} \tag{40}$$

and

$$\nu^e_{xy} = \frac{-\cos\alpha(a + l\cos\alpha_0)}{\sin\alpha(b - l\sin\alpha_0)} \tag{41}$$

From Equations 34 and 37 we have

$$d\varepsilon_x = d\sigma_x Y l^2 \sin^2\alpha/3K_f X \tag{42}$$

yielding a Young's modulus in the x direction due to flexure of the fibrils of

$$E_x = \frac{3K_f}{l^2\sin^2\alpha}\frac{(a + l\cos\alpha)}{(b - l\sin\alpha)} \tag{43}$$

The expression for Young's modulus due to instantaneous changes in engineering stress and strain is found by replacing the unit-cell lengths in Equation 42 with the undeformed unit-cell lengths

$$E^e_x = \frac{3K_f}{l^2\sin^2\alpha}\frac{(a + l\cos\alpha_0)}{(b - l\sin\alpha_0)} \tag{44}$$

The changes in the unit-cell lengths due to flexure under a change $\Delta\sigma_y$ in a y-directed load are also given by Equations 35 and 36 and hence the Poisson's ratio due to a uniaxial stress in the y direction is

$$\nu_{yx} = \frac{-d\varepsilon_x}{d\varepsilon_y} = \frac{-\sin\alpha(b - l\sin\alpha)}{\cos\alpha(a + l\cos\alpha)} \tag{45}$$

and the engineering Poisson's ratio is

$$\nu^e_{yx} = \frac{-\sin\alpha(b - l\sin\alpha_0)}{\cos\alpha(a + l\cos\alpha_0)} \tag{46}$$

The component of force causing flexure due to a y-directed load (see Fig. 2d) is

$$\Delta F = \Delta F_y \cos\alpha/2 = \Delta\sigma_y X\cos\alpha/2 \tag{47}$$

Substituting Equations 29, 33 and 47 into Equation 28 yields

$$\Delta f = \frac{\Delta\sigma_y X l^2\cos\alpha}{6K_f} \tag{48}$$

From Equations 38 and 48 we find

$$d\varepsilon_y = d\sigma_y X l^2\cos^2\alpha/3K_f Y \tag{49}$$

in the limit of infinitesimal changes in applied load. Hence the Young's modulus in the y direction due to flexure is

$$E_y = d\sigma_y/d\varepsilon_y = \frac{3K_f}{l^2\cos^2\alpha}\frac{(b - l\sin\alpha)}{(a + l\cos\alpha)} \tag{50}$$

The engineering Young's modulus in the y direction is simply

$$E_y^e = \frac{3K_f}{l^2\cos^2\alpha}\frac{(b - l\sin\alpha_0)}{(a + l\cos\alpha_0)} \quad (51)$$

In the analysis of the elastic properties of a honeycomb network [19] the deformation is considered to be due to flexure of the diagonal honeycomb cell walls of length, l, thickness, t, depth, w, and intrinsic Young's modulus, E_s. This is exactly equivalent to the deformation of the node–fibril network of Fig. 1a due to flexure of the (diagonal) fibrils. The elastic moduli of a honeycomb network deforming due to flexure are [19]

$$\nu_{xy} = \nu_{yx}^{-1} = \frac{\cos\beta}{\sin\beta}\frac{X}{Y} \quad (52)$$

$$E_x = \left(E_s\frac{wt^3}{l}\right)\left(\frac{X}{l^2ZY\sin^2\beta}\right) \quad (53)$$

$$E_y = \left(E_s\frac{wt^3}{l}\right)\left(\frac{Y}{l^2ZX\cos^2\beta}\right) \quad (54)$$

where β is the honeycomb angle (equivalent to α), X and Y are the unit-cell lengths (equivalent to, though not the same as, Equations 3 and 4, respectively), and Z is the depth of the unitcell which, for honeycombs, is equal to the depth of the cell wall, w. For comparison of the elastic moduli expressions for the honeycomb and NF models it is necessary to use expressions for a re-entrant honeycomb, i.e. $\beta = -\alpha$ in Equations 52–54. Substituting Equations 3 and 4 into Equations 40 and 45 then yields identical NF model expressions to the honeycomb model Poisson's ratios of Equation 52.

The NF model Young's moduli were derived for a unit thickness of the unit cell perpendicular to the x–y plane. However, it is easily shown that for an arbitrary unit-cell depth of Z, the NF model Young's moduli become

$$E_x = 3K_f\left(\frac{X}{l^2ZY\sin^2\alpha}\right) \quad (55)$$

and

$$E_y = 3K_f\left(\frac{Y}{l^2ZX\cos^2\alpha}\right) \quad (56)$$

Comparison of the Young's moduli in the two models (Equation 55 with Equation 53, and Equation 56 with Equation 54 yields)

$$K_f = E_s wt^3/3l \quad (57)$$

Hence the flexure force coefficient is a function of the intrinsic fibril Young's modulus, E_s, and the fibril dimensions. Note that, whereas $Z = w$ in the honeycomb model, this is not necessarily the case in the NF model, because Z will depend on the node–fibril microstructure in the z direction.

The expressions for the elastic moduli due to fibril flexure in the NF model are also included in Table I. It is to be noted that the Poisson's ratios due to flexure are identical to those due to hinging of the fibrils. Similarly, the expressions for the Young's moduli are almost identical between the two deformation mechanisms, differing only by a factor of 3 and the nature of the force coefficients involved. As before, Equations 24 and 25 are satisfied.

2.3. Fibril stretching

We now consider the case of fibrils that are assumed to be extensible rods. Effects due to fibril hinging and flexure will be ignored, i.e. for any fibril angle, α, only the fibril length will be allowed to vary, with the fibril remaining straight always. Because we are treating the fibrils as elastic rods, we can consider tension in both directions. Compression will also give the same answer.

Fibril extension under a tensile load applied to the node–fibril network in the x direction is illustrated in Fig. 3. The stretching force coefficient is defined from Equation 1 as

$$K_s = \Delta F/\Delta s \quad (58)$$

where ΔF is the change in the component of the load applied along the fibril length and Δs is the axial extension of the fibril.

Consider the axial extension of a fibril at angle α to the x axis due to a small change, $\Delta\sigma_x$, in the applied stress in the x direction. The changes in the unit-cell lengths due to fibril extension are

$$\Delta X = 2\Delta s\cos\alpha \quad (59)$$

$$\Delta Y = -2\Delta s\sin\alpha \quad (60)$$

For an infinitesimal change in applied load then the infinitesimal changes in strain due to fibril stretching are, therefore

$$d\varepsilon_x = 2ds\cos\alpha/X \quad (61)$$

$$d\varepsilon_y = -2ds\sin\alpha/Y \quad (62)$$

From Equations 3, 4, 39, 61 and 62 we find the Poisson's ratio due to fibril stretching under a uniaxial applied stress along the x direction is

$$\nu_{xy} = \frac{\sin\alpha(a + l\cos\alpha)}{\cos\alpha(b - l\sin\alpha)} \quad (63)$$

Similarly, substituting the initial unit-cell lengths X_0 and Y_0 for X and Y, respectively, in Equations 61 and 62 we find

$$\nu_{xy}^e = \frac{\sin\alpha(a + l\cos\alpha_0)}{\cos\alpha(b - l\sin\alpha_0)} \quad (64)$$

The component, ΔF, along each fibril of the change in applied force $\Delta F_x/2$ is

$$\Delta F = \Delta F_x\cos\alpha/2 \quad (65)$$

TABLE I Poisson's ratio, engineering Poisson's ratio. Young's modulus and engineering Young's modulus expressions for the hinging, flexure and stretching modes of deformation in the NF model for microporous polymers assuming the fibrils act as rods

	Hinging	Flexure	Stretching
ν_{xy}	$\frac{-\cos\alpha(a+l\cos\alpha)}{\sin\alpha(b-l\sin\alpha)}$	$\frac{-\cos\alpha(a+l\cos\alpha)}{\sin\alpha(b-l\sin\alpha)}$	$\frac{\sin\alpha(a+l\cos\alpha)}{\cos\alpha(b-l\sin\alpha)}$
ν^{e}_{xy}	$\frac{-\cos\alpha(a+l\cos\alpha_0)}{\sin\alpha(b-l\sin\alpha_0)}$	$\frac{-\cos\alpha(a+l\cos\alpha_0)}{\sin\alpha(b-l\sin\alpha_0)}$	$\frac{\sin\alpha(a+l\cos\alpha_0)}{\cos\alpha(b-l\sin\alpha_0)}$
ν_{yx}	$\frac{-\sin\alpha(b-l\sin\alpha)}{\cos\alpha(a+l\cos\alpha)}$	$\frac{-\sin\alpha(b-l\sin\alpha)}{\cos\alpha(a+l\cos\alpha)}$	$\frac{\cos\alpha(b-l\sin\alpha)}{\sin\alpha(a+l\cos\alpha)}$
ν^{e}_{yx}	$\frac{-\sin\alpha(b-l\sin\alpha_0)}{\cos\alpha(a+l\cos\alpha_0)}$	$\frac{-\sin\alpha(b-l\sin\alpha_0)}{\cos\alpha(a+l\cos\alpha_0)}$	$\frac{\cos\alpha(b-l\sin\alpha_0)}{\sin\alpha(a+l\cos\alpha_0)}$
E_x	$\frac{K_h(a+l\cos\alpha)}{l^2\sin^2\alpha(b-l\sin\alpha)}$	$\frac{3K_f(a+l\cos\alpha)}{l^2\sin^2\alpha(b-l\sin\alpha)}$	$\frac{K_s(a+l\cos\alpha)}{\cos^2\alpha(b-l\sin\alpha)}$
E^{e}_x	$\frac{K_h(a+l\cos\alpha_0)}{l^2\sin^2\alpha(b-l\sin\alpha_0)}$	$\frac{3K_f(a+l\cos\alpha_0)}{l^2\sin^2\alpha(b-l\sin\alpha_0)}$	$\frac{K_s(a+l\cos\alpha_0)}{\cos^2\alpha(b-l\sin\alpha_0)}$
E_y	$\frac{K_h(b-l\sin\alpha)}{l^2\cos^2\alpha(a+l\cos\alpha)}$	$\frac{3K_f(b-l\sin\alpha)}{l^2\cos^2\alpha(a+l\cos\alpha)}$	$\frac{K_s(b-l\sin\alpha)}{\sin^2\alpha(a+l\cos\alpha)}$
E^{e}_y	$\frac{K_h(b-l\sin\alpha_0)}{l^2\cos^2\alpha(a+l\cos\alpha_0)}$	$\frac{3K_f(b-l\sin\alpha_0)}{l^2\cos^2\alpha(a+l\cos\alpha_0)}$	$\frac{K_s(b-l\sin\alpha_0)}{\sin^2\alpha(a+l\cos\alpha_0)}$

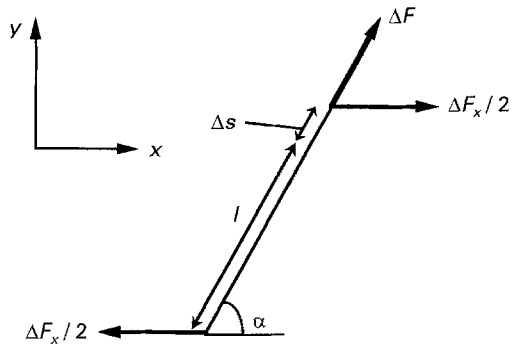

Figure 3 Fibril extension under tension of the NF network in the x direction.

where ΔF_x is given by Equation 7. From Equations 7, 58 and 65 we find, for an infinitesimal change in applied load that Equation 61 becomes

$$d\varepsilon_x = d\sigma_x Y \cos^2\alpha / K_s X \tag{66}$$

Hence the Young's modulus of the NF model due to fibril extension under an applied load in the x direction is

$$E_x = \frac{K_s}{\cos^2\alpha}\frac{(a+l\cos\alpha)}{(b-l\sin\alpha)} \tag{67}$$

Once again, substituting the undeformed unit-cell lengths for the deformed lengths enables the engineering Young's modulus due to fibril stretching to be derived

$$E^{e}_x = \frac{K_s}{\cos^2\alpha}\frac{(a+l\cos\alpha_0)}{(b-l\sin\alpha_0)} \tag{68}$$

Now consider deformation of the unit cell due to a small change, $\Delta\sigma_y$, in an applied stress in the y direction. Equations 61 and 62 again correspond to the infinitesimal changes in strain in the x and y directions due to an infinitesimal change in the applied load. Hence the Poisson's ratio due to a uniaxial stress in the y direction is

$$\nu_{yx} = \frac{\cos\alpha(b-l\sin\alpha)}{\sin\alpha(a+l\cos\alpha)} \tag{69}$$

and the engineering Poisson's ratio is

$$\nu^{e}_{yx} = \frac{\cos\alpha(b-l\sin\alpha_0)}{\sin\alpha(a+l\cos\alpha_0)} \tag{70}$$

The change in the component of a y-directed force acting along the fibril length is

$$\begin{aligned}\Delta F &= -\Delta F_y \sin\alpha/2 \\ &= -\Delta\sigma_y X \sin\alpha/2\end{aligned} \tag{71}$$

In the limit of infinitesimal changes in applied force, Equations 58, 62 and 71 yield

$$d\varepsilon_y = d\sigma_y X \sin^2\alpha / K_s Y \tag{72}$$

and hence the Young's modulus in the y direction due to fibril stretching is

$$E_y = \frac{K_s}{\sin^2\alpha}\frac{(b-l\sin\alpha)}{(a+l\cos\alpha)} \tag{73}$$

and the engineering Young's modulus is

$$E^{e}_y = \frac{K_s}{\sin^2\alpha}\frac{(b-l\sin\alpha_0)}{(a+l\cos\alpha_0)} \tag{74}$$

From Equations 63, 67, 69 and 73 we have

$$\begin{aligned}\nu_{xy}E_y &= \nu_{yx}E_x \\ &= K_s/\sin\alpha\cos\alpha\end{aligned} \tag{75}$$

and

$$|\nu_{xy}| = (E_x/E_y)^{1/2} \tag{76}$$

satisfying both the requirements of a symmetric stiffness matrix and a positive definite strain energy.

3. Results

The expressions for the elastic moduli from the NF model for the hinging, flexure and stretching deformation modes are summarized in Table I. In this section we present the results of model calculations for each of these modes of deformation for the specific loading conditions employed in the experiments on auxetic PTFE [5] and UHMWPE [14, 21]. A comparison of the model predictions is then made with the experimental data for each polymer.

3.1. Model calculations

Fig. 4a and b are plots of the Poisson's ratio and Young's modulus behaviour for each mode of deformation in the NF model with respect to the total true strain in the loading direction for tension along the x axis and compression along the y axis, respectively. These illustrate the highly strain-dependent variations of the properties. Fig. 4a and b correspond to the loading conditions employed in the experimental measurements of the mechanical properties of auxetic PTFE [5] and UHMWPE [14], respectively. For Fig. 4a, ν_{xy} and E_x were calculated using Equations 2 and 14 (hinging), Equations 40 and 43 (flexure), and Equations 63 and 67 (stretching), respectively. For Fig. 4b, ν_{yx} and E_y were calculated using Equations 16 and 22 (hinging), Equations 45 and 50 (flexure), and Equations 69 and 73 (stretching), respectively. The total true strain used in Fig. 4a was calculated by integrating the infinitesimal increment of true strain defined by Equation 13, i.e.

$$\varepsilon_x = \int_{X_0}^{X} \mathrm{d}X/X = \ln(X/X_0) \qquad (77)$$

Substituting Equation 3 into Equation 77 yields

$$\varepsilon_x = \ln[(a + l\cos\alpha)/(a + l\cos\alpha_0)] \qquad (78)$$

Similarly, the total true strain used in Fig. 4b was calculated using

$$\varepsilon_y = \ln[(b - l\sin\alpha)/(b - l\sin\alpha_0)] \qquad (79)$$

Values of α are indicated on the top x axis of Fig. 4a and b.

The following parameters were used in the model calculations of Fig. 4a: $b = 0.2a, l = b/2$ and $\alpha_0 = 90°$. These parameters were chosen in agreement with previous experimental [5] and theoretical [6] works and are consistent with the initial undeformed microstructure being observed to be fully densified due to a preconditioning process [5] prior to testing (Fig. 1b). To ensure the arbitrary dimensions of Young's modulus were compatible for all deformation modes, and to enable comparison of the strain-dependent behaviour, the force coefficients used were as follows: $K_h/l^2 = K_f/l^2 = K_s = 1$.

The ν_{xy} behaviour is identical for the hinging and flexure modes of deformation: $\nu_{xy} = 0$ at $\varepsilon_x = 0$, becoming increasingly negative as ε_x increases until $\varepsilon_x = 0.095$ (i.e. $\alpha = 0°$) where ν_{xy} is infinitely negative.

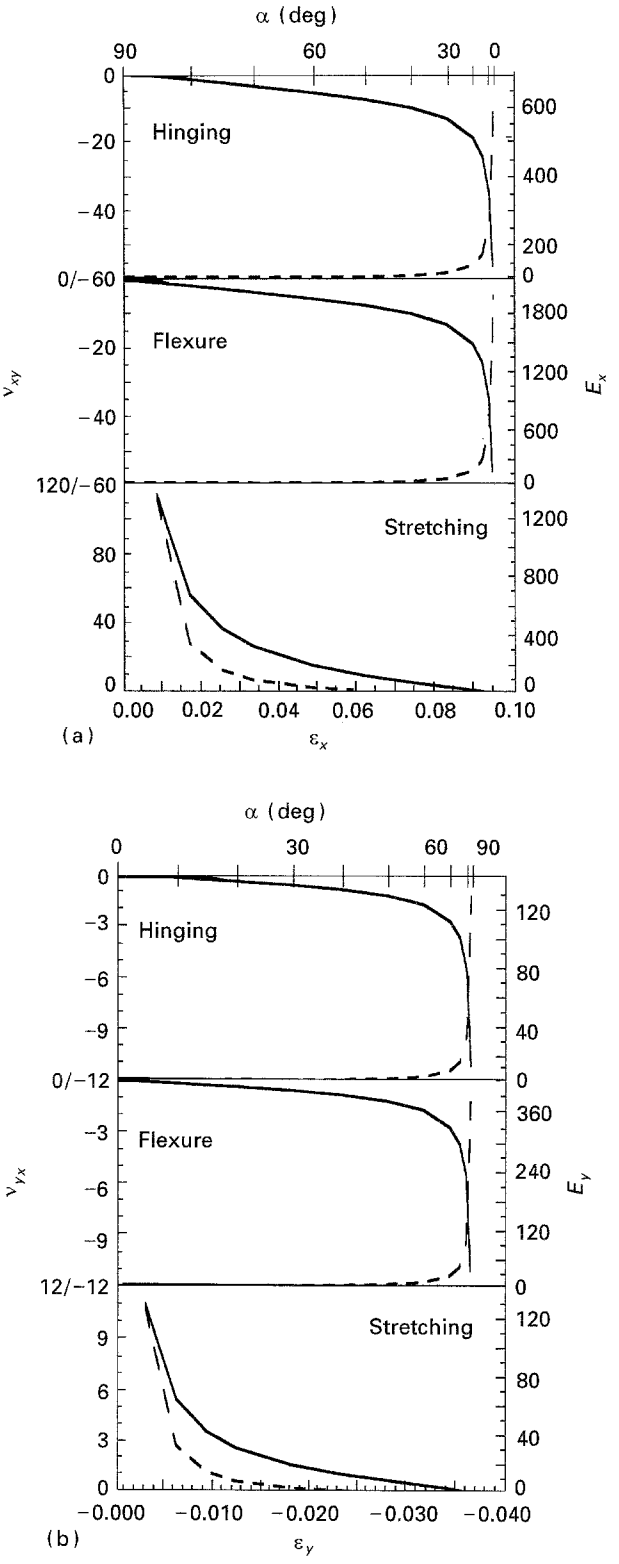

Figure 4 (a) NF model (——) ν_{xy} and (– – –) E_x versus ε_x curves for hinging, flexure and stretching modes of deformation. $b/a = 0.2$, $l = 0.1\,a$ and $\alpha_0 = 90°$ with $K_h/l^2 = K_f/l^2 = K_s = 1$. Corresponding values of α are indicated along the top x axis. (b) NF model (——) ν_{yx} and (– – –) E_y versus ε_y curves for hinging, flexure and stretching modes of deformation. $b = a$, $l = 0.036\,a$ and $\alpha_0 = 0°$ with $K_h/l^2 = K_f/l^2 = K_s = 1$.

The stretching mode of deformation shows markedly different behaviour: ν_{xy} is infinite and positive at $\varepsilon_x = 0$, decreasing in magnitude as ε_x increases until the final strain where $\nu_{xy} = 0$.

The E_x trends for hinging and flexure are also identical, differing only in magnitude by a factor of 3 for

the values of K_h and K_f employed here (see Table I and Equations 15 and 44). For both modes, E_x has a relatively small finite value at $\varepsilon_x = 0$, increasing slowly as ε_x increases until ε_x approaches 0.095 where E_x undergoes a dramatic increase tending towards infinity at $\varepsilon_x = 0.095$. Once again the stretching mode shows markedly dissimilar behaviour: E_x is infinite at $\varepsilon_x = 0$ (due to the fibrils being oriented perpendicular to the loading direction in this case and hence stretching along the fibril length cannot occur), decreasing to a relatively small finite value at the final strain.

The parameters employed in the model calculations for Fig. 4b were $a = b$, $l = 0.036b$ and $\alpha_0 = 0°$, as used in [14]. Once again Young's modulus compatibility was ensured by using $K_h/l^2 = K_f/l^2 = K_s = 1$.

The ν_{yx} curves for hinging and flexure are identical, with $\nu_{yx} = 0$ at $\varepsilon_y = 0$, slowly becoming increasingly negative as the strain increases until ε_y approaches -0.037 (i.e. α tends to 90°) where ν_{yx} rapidly tends to an infinitely large negative value. For the stretching mode of deformation, ν_{yx} is infinite and positive at $\varepsilon_y = 0$, rapidly decreasing to a small positive value as the compressive strain increases slightly, followed by a slowly decreasing tail for the remainder of the strain until $\nu_{yx} = 0$ at $\varepsilon_y = -0.037$ ($\alpha = 90°$).

The Young's modulus curves for hinging and flexure follow identical trends, E_y being small and finite at $\varepsilon_y = 0$, increasing slowly with increasing compressive strain until a rapid increase to infinity is observed as ε_y approaches -0.037. The stretching mode of deformation exhibits the opposite Young's modulus behaviour, E_y being infinite at $\varepsilon_y = 0$, rapidly decreasing as the compressive strain increases slightly, followed by a long tail off to a relatively small finite value at $\varepsilon_y = -0.037$ ($\alpha = 90°$). Once again we see that hinging and flexure are easier to achieve when the fibrils are aligned normal to the loading direction than when they are parallel to the loading direction, whereas stretching occurs more readily when the fibrils are aligned along the loading direction than when they are perpendicular to the loading direction.

3.2. Comparison with experimental data

In this section we establish the best-fit model parameters for both PTFE and UHMWPE and compare the model strain-dependent elastic moduli with the known experimental data for these two polymers.

3.2.1. PTFE

3.2.1.1. Obtaining the geometric variables. The variables in the model are the initial fibril angle, α_0, nodule aspect ratio, a/b, and fibril length, l. If we assume, for now, that the experimental preconditioning process applied to the PTFE specimen leaves the initial microstructure in the closest possible packing then $\alpha_0 = 90°$ and $l = b/2$; see Fig. 1b. From Fig. 4a we see that the Young's modulus due to stretching is at its highest value at $\alpha = 90°$ whereas the Young's moduli due to hinging or flexure are at their lowest values. Hence at high values of α the stretching mode will be unfavoured energetically due to it having a higher strain energy (which is proportional to the Young's modulus) associated with it. Experimentally the fibrils were observed to align themselves along the loading direction as the loading strain increased. Furthermore, the fibrils were observed to remain taut throughout. Hence we shall assume that the deformation observed at the lower end of the strain range covered experimentally is predominantly due to hinging. (Because the elastic moduli due to both hinging and flexure have identical strain-dependent behaviour (Fig. 4) the distinction between hinging and flexure is not critical in fixing the parameters to be employed in the model.)

In Fig. 5a we plot the model ν_{xy} versus ε_x curves for $b/a = 0.2$, 0.25 and 0.3 with $l = b/2$ and $\alpha_0 = 90°$ in each case for the hinging mode of deformation in the NF model (calculated from Equations 2 and 78). For comparison the experimental data points up to $\varepsilon_x = 0.15$ are also plotted. An aspect ratio of $b/a = 0.25$ provides an excellent fit to the experimental data up to $\varepsilon_x \sim 0.10$. The value of l determines where the model ν_{xy} curve tends to an infinitely negative value for a given value of a (i.e. at $\alpha = 0°$: $\nu_{xy} = -\infty$, Equation 2, at $\varepsilon_x = \ln[(a + l)/a]$, Equation 78). Hence the $b/a = 0.2$ ($l = 0.1a$) curve tends to $\nu_{xy} = -\infty$ at a lower strain than the $b/a = 0.25$ ($l = 0.125a$) curve which, in turn, tends to $\nu_{xy} = -\infty$

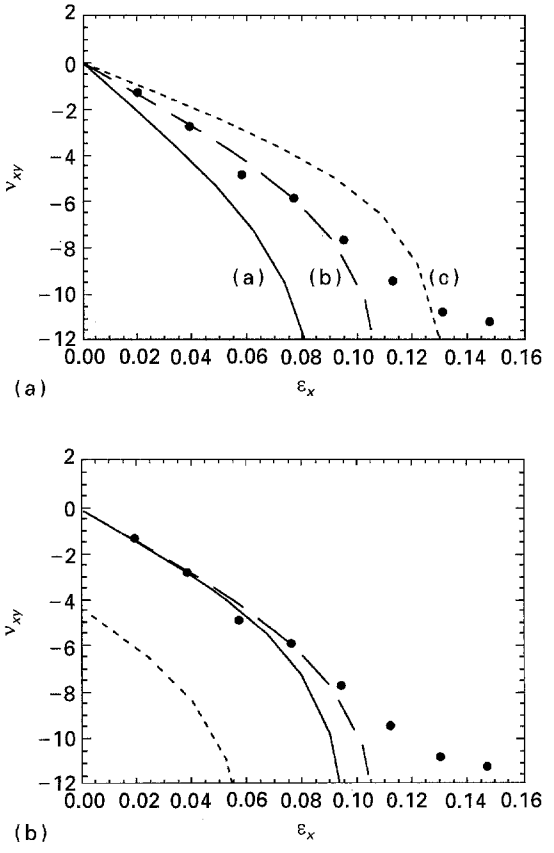

Figure 5 (a) NF model ν_{xy} versus ε_x curves for the hinging mode of deformation in the NF model. Fits are for (*a*) $b/a = 0.2$, (b) 0.25 and (c) 0.3 with $l = b/2$ in all cases, Experimental data points (●) for PTFE are also shown for comparison. (b) NF model ν_{xy} versus ε_x curves for the hinging mode of deformation in the NF model. Curves are for $b/a = 0.25$ with $l =$ (——) $0.11a$ ($< b/2$), (– – –) $0.125a$ ($= b/2$), and (- - - -) $0.14a$ ($> b/2$). Experimental data points (●) for PTFE are also shown for comparison.

at a lower strain than the $b/a = 0.3$ ($l = 0.15a$) curve. From SEM observation $b/a \sim 0.2 - 0.25$ is reported [6] to be a typical nodule aspect ratio range for the PTFE specimens which is in agreement with the $b/a = 0.25$ model fit to the data in this case.

For the $b/a = 0.25$ curve in Fig. 5a, the fit between $0.10 < \varepsilon_x \leq 0.12$ rapidly deteriorates as ε_x increases. However, in this strain range, α approaches 0° and, therefore, we might expect the fibril stretching mode of deformation to become important as the fibrils become aligned along the loading direction. Considering the simplicity of the model, the fit of the $b/a = 0.25$ ν_{xy} versus ε_x curve to the experimental data for $\varepsilon_x < 0.10$ is excellent.

Now consider the situation where $l \neq b/2$. For $l < b/2$ then the closest packed (initial) microstructure is as shown schematically in Fig. 1c. Once again $\alpha_0 = 90°$ and Equations 2 and 78 yield $\nu_{xy} = 0$ at $\varepsilon_x = 0$ due to hinging. However, for $l > b/2$ then Fig. 1d is the closest packing (i.e. initial/undeformed) microstructure and hence Equation 78 yields the model ε_x values with $\alpha_0 = \alpha_c$, where α_c is given by

$$\sin\alpha_c = b/2l \tag{80}$$

Because $\alpha_0 < 90°$ then, for hinging, $\nu_{xy} < 0$ at $\varepsilon_x = 0$ (se Equation 2 and Fig. 4a).

Fig. 5b compares the NF model ν_{xy} versus ε_x curves due to hinging for $b/a = 0.25$ and $l = 0.125a$ ($= b/2$), $0.11a$ ($< b/2$), $0.14a$ ($> b/2$). The experimental data up to $\varepsilon_x = 0.15$ for PTFE are also included for comparison. The experimental data points appear to extrapolate back to $\nu_{xy} \sim 0$ at $\varepsilon_x = 0$. Hence the model curve for $l > b/2$ (i.e. $l = 0.14a$ in this case) does not give the correct trend because $\nu_{xy} < 0$ at $\varepsilon_x = 0$ (i.e. $\nu_{xy} = -4.3$ at $\varepsilon_x = 0$ in Fig. 5b). For $l = 0.11a$ (i.e. $l < b/2$) the model ν_{xy} curve gives good agreement at low ε_x values but the agreement deteriorates at a lower strain ($\varepsilon_x \sim 0.08$) than for the $l = 0.125a$ (i.e. $l = b/2$) curve ($\varepsilon_x \sim 0.10$). Hence we conclude that the curve with $l = b/2$ is the best fit of the model to the PTFE data for an aspect ratio of $b/a = 0.25$. This is in agreement with experimental observation [5] of full densification in the undeformed condition.

3.2.1.2. Comparison of elastic moduli with model. The Poisson's ratio, ν_{xy}, and engineering Young's modulus, E_x^e, data from [5] are plotted against the total true strain in the loading (x) direction, ε_x, in Fig. 6a and b, respectively. The data show three distinct regions of deformation behaviour. Region I ($0 < \varepsilon_x < 0.15$) is a low Young's modulus region in which the Poisson's ratio value is negative, increasing in magnitude as the strain increases until a maximum negative value of $\nu_{xy} \sim -11$ is achieved at $\varepsilon_x = 0.15$. In region II ($0.15 < \varepsilon_x < 0.215$) the Young's modulus shows a steep increase, eventually achieving a plateau at the higher strain range in this region. The value of the Poisson's ratio in this region decreases in magnitude to $\nu_{xy} \sim 0$ at $\varepsilon_x = 0.215$. Region III ($0.215 < \varepsilon_x < 0.29$) shows a steep decrease in Young's modulus followed by a tailing off to $E_x^e \sim 0$ at $\varepsilon_x = 0.29$. The Poisson's ratio for region III goes positive and remains at a constant value ($\nu_{xy} \sim 1.2$) for $\varepsilon_x > 0.23$. A maximum uncertainty in the ν_{xy} data of 8% is quoted in [5].

In an earlier work it was suggested that nodule rotation was required to explain the modulus and Poisson's ratio curves beyond region I of Fig. 6. In this model the fibrils were treated as inextensible rods. With the addition of deformation of the fibrils themselves, a more realistic scenario, it is possible to describe the full shape of the curves without the need for nodule rotation. In this case, for α near 90° the deformation mode is predominantly fibril hinging or flexure, with fibril stretching taking over as $\alpha \to 0°$. In reality these mechanisms will exist concurrently but for simplicity we shall consider them occurring consecutively.

In this new scenario, then, region I of Fig. 6 is due to nodule translation due to fibril hinging, region II due to elastic fibril stretching and region III due to plastic deformation of the fibrils. If the physical origin of the hinging force coefficient is due to friction between nodule particles, as suggested in [5], then this hinging-plus-stretching NF model is consistent with experimental observation [5] where the deformation during region I of Fig. 6 is apparently inelastic, that during region II is linearly elastic and in region III the material deforms plastically.

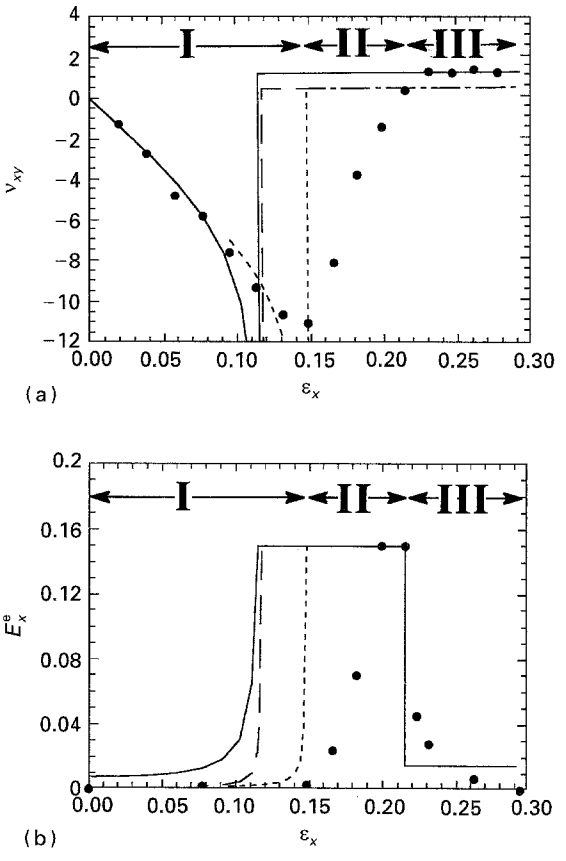

Figure 6 (a) Experimental ν_{xy} versus ε_x data (●) for PTFE. (b) Experimental E_x^e versus ε_x data (●) for PTFE. Also shown are NF (hinging-plus-stretching) model calculations for $b = 0.25a$, $l = b/2$ and $\alpha_0 = 90°$. (——) the fit to the ν_{xy} data, (— — —) the fit to the E_x^e data. (– – –) NF model calculations for $b = 0.25a$, $l = 0.16a$ and $\alpha_0 = 90°$, from fit to the E_x^e data. All NF model E_x^e predictions were normalized to the peak experimental E_x^e value of $E_x^e = 0.15$ GPa.

The transition strain from fibril hinging to stretching will be considered to occur at a fibril angle of α_s, the value of α at which the engineering Young's moduli due to hinging and stretching are equal. From Fig. 4a it is clear that the modulus due to hinging is less than that due to stretching for $\alpha > \alpha_s$ and, therefore, hinging will be presumed to be the only deformation mode in this simplistic scenario. At α_s, hinging ceases, because the modulus due to stretching would be lower than that due to hinging for any further decrease in α. α_s is, therefore, the final fibril angle, with further deformation thereby due to fibril stretching. The transition from elastic to plastic fibril extension is described by a decrease in the value of the stretching force coefficient, K_s.

Equating Equations 15 and 68 we see that α_s is related to the appropriate force coefficients by

$$\tan^2\alpha_s = K_h^{eff}/K_s \tag{81}$$

where K_h^{eff} is an effective hinging force coefficient defined as

$$K_h^{eff} = K_h/l^2 \tag{82}$$

Hence, the value of K_h^{eff}/K_s fixes the value of α_s and vice versa.

Two methods were used to determine the value of α_s to be used in the NF model calculations for PTFE. In the first method the value of α_s was fixed by requiring $\nu_{xy} \sim +1.2$ due to fibril extension (Equation 63). This is the experimentally observed value of the Poisson's ratio in region III, which is assumed to correspond to plastic extension of the fibrils, i.e. hinging has ceased in this region and, therefore, $\alpha = \alpha_s$. This yields $\alpha_s \sim 13°$ for the previously determined best-fit nodule/fibril dimensions of $b = 0.25a$ and $l = b/2$. The NF model Poisson's ratio and engineering Young's modulus calculations for $b = 0.25a$, $l = b/2$, $\alpha_0 = 90°$ and $\alpha_s = 13°$ are included in Fig. 6a and b, respectively. In the calculations the elastic moduli due to hinging (Equations 2 and 15) were used for $\alpha > \alpha_s$ (i.e. $\varepsilon_x < 0.115$ for $\alpha_s = 13°$), and the elastic moduli due to stretching (Equations 63 and 68) were used for $\alpha = \alpha_s$. The X unit-cell length during fibril extension at α_s is given by

$$X = a + (l + \Delta s)\cos\alpha_s \tag{83}$$

where Δs is the fibril extension. Substituting Equation 83 into Equation 77 yields the model expression used to calculate the total true strain in the loading direction during the fibril extension phase

$$\varepsilon_x = \ln\{[a + (l + \Delta s)\cos\alpha_s]/(a + l\cos\alpha_0)\} \tag{84}$$

In Fig. 6b the NF model Young's modulus data due to elastic fibril stretching were normalized to the peak value in the experimental data (0.15 GPa). Plastic deformation was modelled by decreasing the value of K_s by an arbitrary factor of 10 at the experimentally observed transition strain from region II to III of $\varepsilon_x = 0.215$.

In the second method used to calculate α_s, the experimental Young's modulus data at $\varepsilon_x \sim 0.08$ and $\varepsilon_x \sim 0.215$ were assumed to be due to fibril hinging and elastic stretching, respectively. Assuming $l = 0.125a$ (i.e. $b/2$) and $\alpha_0 = 90°$ then the value of the fibril angle during hinging at $\varepsilon_x \sim 0.08$ is calculated from Equation 78 as $\alpha \sim 50°$. From Equations 15, 68 and 82 we have

$$\frac{E_x^e(\alpha = 50°)}{E_x^e(\alpha_s)} = \frac{K_h^{eff}}{\sin^2(50°)}\frac{\cos^2\alpha_s}{K_s} \tag{85}$$

where $E_x^e(\alpha = 50°)$ (~ 0.002 GPa) and $E_x^e(\alpha_s)$ (~ 0.150 GPa) are the experimental engineering Young's moduli at $\varepsilon_x \sim 0.08$ and 0.215, respectively. Assuming α_s is close enough to 0° so that $\cos^2\alpha_s$ can be considered equal to unity gives $K_s/K_h^{eff} \sim 128$. Hence, from Equation 81 we have $\alpha_s \sim 5°$. The long-dashed lines in Fig. 6a and b correspond to the NF model calculations with $\alpha_s = 5°$. All other model parameters were the same as in the calculations for $\alpha_s = 13°$.

The two NF model calculations yield similar results which, considering the simplicity of the model, would appear to indicate that the two independently determined values of α_s are in reasonable agreement with each other.

Comparison of the model and experimental data of Fig. 6a and b shows that many of the features observed experimentally are now predicted by the model. In particular, the Young's modulus peak is at a higher strain range than the maximum negative value ν_{xy}. The lower strain limit of the E_x^e peak is seen to correspond to the onset of fibril extension and also the rise in the modulus due to hinging as α approaches 0°. The upper strain limit of the E_x^e peak simply corresponds to the strain at which plastic fibril deformation commences.

Fig. 6a illustrates that when stretching becomes the dominant deformation mode ν_{xy} becomes positive and almost constant with strain for $l \ll a$ (because α remains constant in this case – see Equation 63). This is observed experimentally where, in regions II and III, ν_{xy} goes from a large negative value to a constant small positive value at the higher strains.

3.2.2. UHMWPE

The experimental ν_{yx} versus ε_y^c data for UHMWPE under compression (i.e. $\varepsilon_y^c = -\varepsilon_y$) in the y direction are plotted in Fig. 7. The experimental data can be divided into two distinct regions. In region I ($\varepsilon_y^c < 0.0367$) ν_{yx} has a small negative value at the lower strains, increasing slowly with strain at intermediate strains before increasing rapidly in magnitude to $\nu_{yx} \sim -15$ at the highest strains. At the transition from region I to region II ($\varepsilon_y^c = 0.0367$), ν_{yx} assumes a large positive value ($\nu_{yx} \sim +6$) which decreases with increasing strain to $\nu_{yx} \sim 0$ at $\varepsilon_y^c = 0.05$. For $\varepsilon_y^c > 0.05$ the experimental data indicate $\nu_{yx} \sim 0$.

No Young's modulus data are available for this UHMWPE data set. Owing to the much higher stiffness of the auxetic UHMWPE specimen, there was no need to precondition the sample prior to testing.

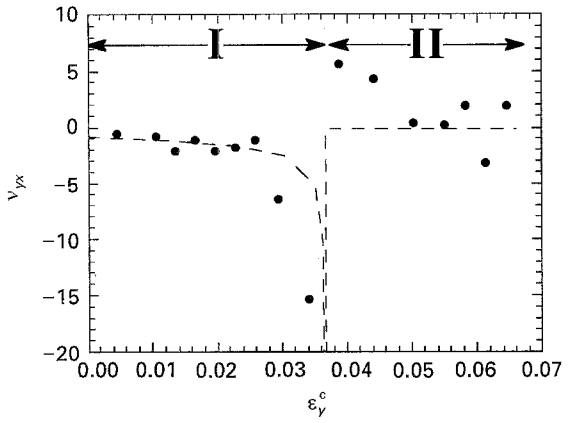

Figure 7 Experimental ν_{yx} versus ε_y^c data for UHMWPE [21] (●). Also shown are NF (hinging-plus-stretching) model calculations for $a = b$ and $\alpha_0 = 40°$ for $l = 0.095b$ (– – –).

The final stage of the fabrication of the sample of UHMWPE used by Neale *et al.* [14] involves extrusion of the material through a die [7] and it was noted that the material expanded in the radial direction (x direction in Fig. 1) on leaving the die. Hence for UHMWPE the initial undeformed structure consists of fully expanded material with fibrils lying in the x direction when $\alpha_0 = 0°$. This is the value of α_0 used by Neale *et al.* [14], where a simple hinging model is found to produce the observed trends of ν_{yx} in region I of Fig. 7, but fails to describe the behaviour in region II.

The value of ε_y^c at the boundary between regions I and II in Fig. 7 determines the ratio of l/b, for any given initial fibril angle α_0, to be employed in the NF model, because $\alpha = 90°$ at this point (if full hinging is assumed to occur), see Equation 79. The major-to-minor nodule axes ratio is found to be typically $a/b = 1$ for UHMWPE [13, 14]. The NF model curves for $a = b, l = 0.036b$ and $\alpha_0 = 0°$ have already been presented in Fig. 4b where it is seen that the hinging and flexure Poisson's ratio predictions show the trends observed in region I of the experimental data of Fig. 7. However, $\alpha_0 = 0°$ yields $\nu_{yx} = 0$ at $\varepsilon_y = 0$ whereas experimentally the data indicate $\nu_{yx} < 0$ at $\varepsilon_y = 0$. This implies $\alpha_0 > 0°$ in the undeformed state. Fig. 7 shows the NF model ν_{yx} versus ε_y^c curve for $a = b$, $l = 0.095b$ and $\alpha_0 = 40°$. This choice of parameters is consistent with typical nodule axes ratios observed for UHMWPE and ensures a transition strain of $\varepsilon_y^c = 0.0367$ where for $\varepsilon_y^c < 0.0367$ deformation is due to fibril hinging, and for $\varepsilon_y^c > 0.0367$ deformation is due to fibril stretching. With these parameters the model follows the trends of the experimental ν_{yx} data very closely, i.e. a small negative value increasing slowly with strain until ε_y^c approaches 0.0367, whereupon a rapid increase in magnitude towards a large negative value is observed at $\varepsilon_y^c = 0.0367$. An initial fibril angle of $\alpha_0 = 40°$ indicates that the material is not in the fully expanded condition in the undeformed state. This is in agreement with other forms of auxetic UHMWPE fabricated by the same processing route where a value of $\alpha_0 = 30°$ is indicated from the model as a typical initial fibril angle [21].

At $\alpha = 90°$ (i.e. $\varepsilon_y^c = 0.0367$) fibril hinging ceases to be possible under further compression along the y axis. However, because $l \ll b$ in this case, the nodules are only in contact in the x direction. Hence further compression in the y direction leads to fibril stretching (or breaking). This is illustrated in Fig. 1c where it is seen that, for rectangular nodules, fibril extension leads to a change in Y but no change in X. Consequently, $\nu_{yx} = 0$, which is exactly the value of ν_{yx} obtained from Equation 69 due to stretching at $\alpha = 90°$. For $\varepsilon_y^c \geq 0.05$, the experimental data indicate $\nu_{yx} \sim 0$. Hence for $\varepsilon_y^c \geq 0.05$ the experimental data are consistent with deformation due to fibril stretching at $\alpha = 90°$.

We can say, therefore, that the NF model calculations for $a = b$, $l = 0.095b$ and $\alpha_0 = 40°$ give excellent agreement with the experimental Poisson's ratio data in the strain ranges $0 < \varepsilon_y^c < 0.026$ and $0.050 < \varepsilon_y^c < 0.065$ when complete fibril hinging is followed by fibril stretching.

4. Discussion

We have seen that the general features of the experimental ν_{xy} and E_x^c data for PTFE are predicted by the NF model when fibril stretching follows fibril hinging. However, the model calculations in Fig. 6 clearly represent a limiting case. In the real material there will be competition between the hinging and stretching deformation modes throughout the total strain range. In other words, whilst hinging must clearly dominate in the initial stages of the deformation, some fibril stretching will occur. As α approaches 0° fibril stretching will become increasingly dominant. This will have two effects. Firstly, the transition strain between the predominantly hinging and stretching modes will occur at a higher value of strain as a result of the increase in fibril length. Secondly, the transition itself will become smeared over a range of strain. These two effects are observed in the experimental data of Fig. 6 and are currently under investigation both theoretically and experimentally.

The first of these effects is also illustrated in Fig. 6a and b where the NF model calculations for $b = 0.25a$, $\alpha_0 = 90°$ and $l = 0.16a$ are shown with $\alpha_s = 5°$ from the fit to the experimental Young's modulus data (second method). This choice of l produces a value of the transition strain of $\varepsilon_x \sim 0.148$ which is in agreement with the experimental data. Note that no model data with $l = 0.16a$ are included for $\varepsilon_x < 0.095$ in Fig. 6 because this would imply $\alpha > \alpha_c$ (equation 80) and hence is physically meaningless. In Fig. 6a the experimental data initially ($0 \leq \varepsilon_x < 0.10$) follow the model hinging curves for $l = 0.125a$, then in the strain range $0.10 < \varepsilon_x < 0.148$ the experimental data tend towards the model hinging curve with $l = 0.16a$, i.e. fibril stretching becomes significant in this range. At $\varepsilon_x = 0.148$ fibril stretching becomes dominant and the experimental data tend towards the limiting value due to stretching. The effect of increasing the fibril length on the engineering Young's modulus data is seen to be a decrease in the width of the E_x^c peak, due to an increase in the strain at which stretching occurs (see

Fig. 6b), thus improving the agreement with the experimental data.

The general features of the UHMWPE ν_{yx} data are also explained by the hinging-plus-stretching scenario. Improved agreement will also be expected by considering hinging and stretching to act concurrently rather than consecutively. The large positive ν_{yx} values that are observed experimentally at the transition from hinging to stretching are not predicted by the model. Fibril stretching would require $\alpha \sim 10°$ to predict these values whereas $\alpha \sim 90°$ at the transition from hinging to stretching. However, when $\alpha \sim 90°$ the nodules are in close proximity to each other (i.e. the material is densified) and so nodule shape effects may become important at the transition from hinging to stretching. Experimentally, the nodules are observed to be elliptical or circular rather than rectangular [13]. Consequently, when circular nodules, for example, are in contact (analogous to Fig. 1c), hinging ceases. Further compression in the y direction would cause the nodules to move closer together in the y direction and further apart in the x direction, resulting in a positive ν_{yx} value, compared to $\nu_{yx} = 0$ for rectangular nodules. Hence the large positive values may be a result of nodule interactions due to non-rectangular nodule shapes.

In Section 2.2 the fibril flexure force coefficient was found to be related to the Young's modulus of the fibril material and the fibril dimensions by Equation 57. The form of the hinging force coefficient is likely to be complicated, being either due to the friction forces acting between the nodules as suggested for PTFE [5] or due to shearing and polymer-chain alignment effects in the hinge material. We now consider the physical origin of the stretching force coefficient.

Consider the extension, Δs, of a fibril of length, l, thickness, t, depth, w, and Young's modulus, E_s, due to a force, ΔF, applied along the length of the fibril. From Hooke's law

$$E_s = \frac{\sigma}{\varepsilon} = \left(\frac{\Delta F}{wt}\right)\left(\frac{l}{\Delta s}\right) \tag{86}$$

and, therefore, from Equations 58 and 86

$$K_s = E_s w(t/l) \tag{87}$$

Hence the stretching force coefficient is determined by the intrinsic Young's modulus of the material forming the fibril and the fibril dimensions.

Having derived the engineering Young's modulus expression due to fibril stretching in the NF model (Equation 68) and the form of the stretching force coefficient (Equation 87) it is possible to estimate the value of the intrinsic Young's modulus, E_s, of the fibrils during the elastic deformation from the experimental engineering Young's modulus data for PTFE. It is readily shown that in three dimensions Equation 68 becomes

$$E_x^e = \frac{K_s}{\cos^2\alpha}\frac{X_0}{Y_0 Z_0} \tag{88}$$

where X_0, Y_0 and Z_0 are the undeformed unit-cell lengths. From the fits to the ν_{xy} data we have a nodule aspect ratio of $b/a = 0.25$, an initial fibril length of $l_0 = b/2$ and an initial fibril angle of $\alpha_0 = 90°$. These initial parameters are in agreement with experimental observation [5, 6] of a fully densified undeformed microstructure with $a \sim 20$–$25\ \mu m$ and $b \sim 5\ \mu m$. Substituting these initial parameters into Equations 3 and 4 we find

$$X_0 = 8\,Y_0 \tag{89}$$

When the engineering Youngs modulus has achieved its peak value ($E_x^e = 0.15$ GPa) we have $0.199 \leq \varepsilon_x \leq 0.215$ (see Fig. 6b) which from Equation 78 requires l to be approximately double its initial value (due to drawing out of the hinge material) for $\alpha \sim 0°$, i.e.

$$l = 2l_0 = b = Y_0 \tag{90}$$

From SEM examination, the nodules in the real material are observed to be disc-like in shape with diameter, a, and thickness (in the y direction), b [6]. In the absence of any knowledge of the nodule connectivity in the z direction we will assume that the Z_0 unit-cell length corresponds to the diameter of the nodules, i.e.

$$Z_0 = a = 4l \tag{91}$$

For fibrils of equal thickness and width (i.e. $w = t$) then substituting Equations 87, 89, 90 and 91 into Equation 88 yields

$$E_s = \frac{E_x^e}{2}\left(\frac{l}{t}\right)^2 \tag{92}$$

where we have used $\cos^2\alpha \sim 1$ (i.e. $\alpha \sim 0°$) when fibril stretching dominates. In the NF model each nodule has four fibrils attached to it, whereas in the real material many fibrils are observed to be attached to each nodule. Hence the fibril aspect ratio to be employed in the calculations of the fibril Young's modulus is given by

$$(t/l) = \lambda^{1/2}(t_{\text{fibril}}/l) \tag{93}$$

where λ is the ratio of number of fibrils in the real material to number of fibrils in the model, and t_{fibril} is the fibril thickness in the real material. SEM examination [5] indicates $t_{\text{fibril}} \sim 50$ nm and $\lambda = 30 \pm 20$ (i.e. one model fibril corresponds to ~ 30 fibrils in the real material). Hence the range of (t/l) to be employed in Equation 92 is

$$0.03 \leq t/l \leq 0.07 \tag{94}$$

with $(t/l) = 0.055$ for $\lambda = 30$. Substituting $E_x^e = 0.15$ GPa (see Fig. 6b) and Relation 94 into Equation 92 yields a range of values of the Young's modulus of the fibrils for PTFE of $15 \leq E_s \leq 75$ GPa with $E_s = 25$ GPa for $\lambda = 30$.

This range of E_s is much higher than the value of $0.3 < E_s < 0.7$ GPa for bulk PTFE but is of the right order of magnitude for highly ordered PTFE. We have calculated a modulus of $E_s = 288$ GPa at zero strain

and $E_s = 230$ GPa at a tensile strain of 10% along the backbone chain of PTFE using the POLYGRAF molecular modelling program [22], which is a well-established package for predicting a range of properties for polymeric materials. Given that the fibrils will not contain fully ordered PTFE molecules, a range of $15 < E_s < 75$ GPa seems reasonable for the Young's modulus of the single fibrils of PTFE observed in the experimental specimen of [5]. A secant modulus of ~ 1.5 GPa has been reported [23] for PTFE fibres of diameter ~ 0.13 cm. These fibres were themselves noted to be highly fibrous and so they may be considered to be hierarchical structures consisting of three levels: the upper level being the fibres themselves which consist of the intermediate level of fibrils which, in turn, are made up of the lower (atomic) level of PTFE chains.

For the case of UHMWPE, if we take previously reported [24] values of the modulus $0.19 < E_y^e < 0.36$ GPa to be equivalent to the peak (hence stretching modulus) we can determine the value of (t/l) required to produce a given fibril modulus, E_s. The three-dimensional equivalent of Equation 74 is

$$E_y^e = \frac{K_s}{\sin^2\alpha} \frac{Y_0}{X_0 Z_0} \tag{95}$$

where K_s is given by Equation 87 and X_0, Y_0 and Z_0 are the initial unit-cell lengths. From earlier, the best-fit NF model parameters are $a = b$, $l = 0.095b$ and $\alpha_0 = 40°$. Therefore, from Equations 3 and 4 we have $X_0 \sim Y_0$. If we assume that Z_0 is defined by the depth of the nodules then

$$Z = b = 10.5l \tag{96}$$

Hence, assuming $\alpha \sim 90°$, Equation 95 becomes

$$(t/l) = (10.5\, E_y^e/E_s)^{1/2} \tag{97}$$

If the fibrils exhibit a Young's modulus equal to that along the backbone chain of PE (~ 300 GPa [25–28]) then a value of $(t/l) \sim 0.08$ is calculated for $E_y^e \sim 0.2$ GPa. Assuming $\lambda = 30$ (as for PTFE) then the single fibril aspect ratio calculated for UHMWPE is $(t_{fibril}/l) \sim 0.015$ for $E_s = 300$ GPa. Fibril aspect ratios in this range are common in this material [7, 13, 14].

Finally, little has been said of fibril flexure. This is simply because no evidence of it has been observed. While significant changes in fibril angle have been seen at different stages of deformation [5] the fibrils are always observed to be straight. For the strains applied, curvature of the fibrils would be visible if flexing was operating.

5. Conclusion

The general deformation behaviour of microporous PTFE and UHMWPE can be understood in terms of hinging and stretching mechanisms of a node–fibril network microstructure. In this paper we have modelled fibril hinging followed by fibril stretching which results in a sudden change in properties at the transition point. However, the experimental data for PTFE show a transition smeared over a range of strain, indicating that hinging and stretching act concurrently rather than consecutively. For UHMWPE a sharper transition may exist although in this case it is thought that a nodule-shape effect may obscure the transition between hinging and stretching. The dominant mechanism at any strain is governed by the relative force coefficients and fibril orientation at that strain.

Fibril flexure and hinging result in exactly the same Poisson's ratio values and Young's modulus trends. Detailed knowledge of fibril geometry, intrinsic material properties and the mechanism governing hinging are needed to determine the force coefficients involved in the deformation.

The Young's modulus of the fibrils in PTFE has been estimated from the experimental E_x^e data for the PTFE specimen. The fibril modulus is consistent with the fibrils consisting of highly ordered PTFE, as indicated from scanning electron micrographs.

Acknowledgements

The authors acknowledge the support of the Engineering and Physical Sciences Research Council of the United Kingdom. K. E. E. currently holds an EPSRC Advanced Fellowship.

References

1. K. E. EVANS, M. A. NKANSAH, I. J. HUTCHINSON and S. C. ROGERS, *Nature* **353** (1991) 124.
2. A. YEGANEH-HAERI, D. J. WEIDNER and J. B. PARISE, *Science* **257** (1992) 650.
3. N. R. KESKAR and J. R. CHELIKOWSKY, *Nature* **358** (1992) 222.
4. A. ALDERSON and K. E. EVANS (1994) in preparation.
5. B. D. CADDOCK and K. E. EVANS, *J. Phys. D Appl. Phys*, **22** (1989) 1877.
6. K. E. EVANS and B. D. CADDOCK, *ibid.* **22** (1989) 1883.
7. K. L. ALDERSON and K. E. EVANS, *Polymer* **33** (1992) 4435.
8. R. LAKES, *Science* **235** (1987) 1038.
9. K. E. EVANS, M. A. NKANSAH and I. J. HUTCHINSON, *Acta Metall. Mater.* **42** (1994) 1289.
10. K. E. EVANS, *Endeavour* **15** (1991) 170.
11. K. L. ALDERSON, A. P. PICKLES, P. J. NEALE and K. E. EVANS, *Acta Metall. Mater.* **42** (1994) 2261.
12. K. E. EVANS, *Chem. Ind.* **20** (1990) 654.
13. K. L. ALDERSON and K. E. EVANS, *J. Mater. Sci.* **28** (1993) 4092.
14. P. J. NEALE, K. L. ALDERSON, A. P. PICKLES and K. E. EVANS, *J. Mater. Sci. Lett.* **12** (1993) 1529.
15. K. E. EVANS, *J. Phys. D Appl. Phys.* **22** (1989) 1870.
16. B. D. CADDOCK, Private communication (1995).
17. J. E. SHIGLEY, "Applied Mechanics of Materials" (McGraw-Hill, New York, 1976).
18. B. M. LEMPRIERE, *Am. Inst. Aeronaut. Astronaut. J.* **6** (1968) 2226.
19. L. J. GIBSON, M. F. ASHBY, G. S. SCHAJER and C. I. ROBERTSON, *Proc. R. Soc. Lond.* **A382** (1982) 25.
20. R. J. ROARK and W. C. YOUNG, "Formulas for Stress and Strain", 5th Edn (McGraw-Hill, 1976).
21. K. L. ALDERSON and P. J. NEALE Private communication (1994).
22. POLYGRAF, Molecular Simulations Inc., 199 South Los Robles Avenue, Suite 540, Pasadena, CA 91101, USA.
23. R. L. McGEE and J.R COLLIER, *Polym. Eng. Sci.* **26** (1986) 239.

24. K. E. EVANS and K. L. ALDERSON, *J. Mater. Sci. Lett.* **11** (1992) 1721.
25. S. L. HSU and S. KRIMM, *J. Appl. Phys.* **48** (1977) 4013.
26. R. J. SCHAUFELE and T. SHIMANOUCHI, *J. Chem. Phys.* **47** (1967) 3605.
27. L. HOLIDAY and J. W. WHITE, *Pure Appl. Chem.* **26** (1971) 545.
28. "Polygraf User's Manual", Molecular Simulations Inc., 199 South Los Robles Avenue, Suite 540, Pasadena, CA 91101, USA.

Received 18 October 1994
and accepted 20 January 1995